Journal of Molecular Structure 989 (2011) 70–79

Contents lists available at ScienceDirect

Journal of Molecular Structure

journal homepage: www.elsevier.com/locate/molstruc

# Synthesis, molecular structure and spectral analysis: DFT–TDDFT computational study of ruthenium complex of tetradentate *N,N′*-bis(benzimidazole-2yl-ethyl)-ethylenediamine

Hernández J. Guadalupe [a], Jayanthi Narayanan [b], Thangarasu Pandiyan [c,*]

[a] Centro Tecnológico, Facultad de Estudios Superiores (FES-Aragón), Universidad Nacional Autónoma de México (UNAM), Estado de México, CP 57130, Mexico
[b] División de Ingeniería en Informatica, Universidad Politecnica del Valle de México, Av. Mexiquense, Tultitlan, Estado de México, CP 54910, Mexico
[c] Facultad de Química, Universidad Nacional Autónoma de México (UNAM), Ciudad Universitaria, Coyoacán 04510, México D.F., Mexico

ARTICLE INFO

*Article history:*
Received 22 September 2010
Received in revised form 11 January 2011
Accepted 14 January 2011
Available online 23 January 2011

*Keywords:*
DFT
Molecular orbitals
TDDFT
Ruthenium (II)
Benzimidazole

ABSTRACT

Ruthenium complex *of N,N′*-bis(benzimidazol-2-yl-ethyl)ethylenediamine ($L^1$) was prepared and characterized by analytical methods. Structural and spectral properties of *N,N′*-bis(benzimidazol-2-yl-ethyl)ethylenediamine ($L^1$), its dianionic structure ($L^2$), and their complexes such as $[RuL^1Cl(PPh_3)]^+$ and $[RuL^2Cl(PPh_3)]^+$ were studied by DFT. In the structures, the ruthenium ion is positioned in an equatorial plane formed by amine, benzimidazole nitrogens in a distorted octahedral geometry, and chloride and triphenylphospine are axially coordinated. Furthermore, the molecular orbital of $[Ru(L)Cl(PPh_3)]Cl$ ($L = L^1$ or $L^2$) proves that the HOMOs are localized over the benzimidazole and amine moieties, favoring a strong bond with the metal. DFT-TDDFT was used to analyze the molecular orbitals contribution to MLCT bands that were observed in the visible region; interestingly, the calculated spectrum of $[RuL^1Cl(PPh_3)]^+$ qualitatively agrees only with high energy bands (465 nm and 350 nm) of the experimental spectrum, and other visible bands (≈580 and ≈790 nm) observed in the experimental spectrum coincide with the TD-DFT of $[RuL^2(PPh_3)Cl]^+$. However, electrochemical studies show existence of only $[RuL^1Cl(PPh_3)]^+$ in the solution.



## 1. Introduction

Ruthenium(II) complexes are generally stable, diamagnetic, and kinetically inert, and have received great attention for their unparalled photophysical properties because they exhibit interesting chemical and physical behavior; for example, several ruthenium compounds have been proposed as potential anticancer substances [1–4], chemosensors [5,6], and in dye-sensitized solar cells [7,8]. It has been well documented that metal complexes can bind to DNA covalently as well as noncovalently [9–13]. For instance, the complex ImH[*trans*-$RuCl_4$(DMSO)(Im)] (NAMI-A, Im = imidazole) is the first ruthenium complex to enter clinical trials for cancer treatment [1,14], where it has been observed that it has high selectivity for solid tumor metastases [15] (prevents the spread of cancer) and low host toxicity. Furthermore, organometallic ruthenium(II)-arene complexes $[(\eta^6\text{-arene})Ru(II)(en)Cl]^+$ (arene = benzene or benzene derivatives, en = ethylenediamine) have recently been reported as anticancer compounds both in vitro and in vivo studies [16,17].

In the aspect of solar cells, *cis*-dithiocyanatobis-(2,2′-bipyridyl-4,4′-dicarboxylic acid)ruthenium(II) is one of the most efficient heterogeneous charge transfer sensitizers and is widely used in the $TiO_2$-based dye-sensitized solar cell [6,18–26]. The ruthenium polypyridine octahedral complexes are widely used as dyes in dye-sensitized solar cells; the use of ruthenium metal is particularly attractive because in its octahedral coordination geometry, one can introduce specific ligands in a controlled manner to tune photophysical, photochemical, and electrochemical properties [27]. The main feature of the ruthenium compounds is that they can be used as chromophores to produce solar energy because they absorb light in the visible region through metal-to-ligand charge-transfer (MLCT). Therefore, for the mechanistic details of the photo-catalyst function and for the design of efficient molecular devices related to solar energy conversion, understanding the electronic excited states in ruthenium complexes is crucially important. Thus, the development of ruthenium complexes that exhibit the MLCT bands at extended absorption (low energy region) is a challenging research topic.

Although extensive studies have been made on ruthenium compounds containing polypyridyl ligands [6,18–26], the reports on ruthenium compounds containing benzimidazole is limited even though benzimidazole and amine can stabilize ruthenium(II)

* Corresponding author. Tel.: +52 55 56223499.
*E-mail address:* pandiyan@servidor.unam.mx (T. Pandiyan).

0022-2860/$ - see front matter © 2011 Elsevier B.V. All rights reserved.
doi:10.1016/j.molstruc.2011.01.005

because of their moderate π-acceptor amine and π-donor benzimidazole nitrogens. Additionally, the complexes of benzimidazole derived ligands with many transition metal ions have been studied in detail [28–33], but ruthenium compounds using with *N,N′*-bis (benzimidazole-2yl-ethyl)ethylendiamine ($L^1$) do not appear in the literature. Therefore, the present study deals with the geometrical and spectral analyses of the new compound $[Ru(L^1)Cl(PPh_3)]Cl$. To determine the structural and spectral parameters, DFT–TDDFT method is employed to interpret how the chloride and triphenylphosphine are stabilized in the coordination sphere of the complex along with the ligand.

## 2. Experimental/computational details

### 2.1. Materials

All commercially available reagents employed were: ethylenediamine (99%), acrylamide, 1,2-phenylenediamine (99.5%), triphenylphosphine (99%), ruthenium chloride hydrate ($RuCl_3{\cdot}xH_2O$) (Aldrich); tetrabutylammonium hexaflorophosphate (Smith) was re-crystallized twice from aqueous ethanol.

### 2.2. Physical measurements

On a Fisons (Model EA 1108 CHNSO), elemental analyses for the compounds were carried out. $^1H$, $^{13}C$ and $^{31}P$ NMR spectra were recorded for the compounds on Varian Gemini (300 MHz) by using TMS as an internal standard and GC–MS was recorded with a Joel JMS-Axsosha instrument. Electronic spectra were measured for the ruthenium complex in methanol as well as in dichloromethane by a Perkin–Elmer Lambda-900 double beam UV/Vis/NIR spectrophotometer to see the solvents effect.

### 2.3. Computational procedure

By employing the Gaussian-09 program [34], the DFT calculations were performed for *N,N′*-bis (benzimidazole-2yl-ethyl)ethylenediamine) ($L^1$), and its dianionic structure ($L^2$) i.e., after removing hydrogen atom from secondary amine nitrogens. Furthermore, the calculations were carried out with spin unrestricted orbitals for $[RuL^1Cl(PPh_3)]^+$ and $[RuL^2Cl(PPh_3)]^-$. The exchange correlation was treated at the B3LYP [35,36] and the choice of this method was based on the results obtained from 6-31G** used for C, N, Cl, P, and H atoms, and for $Ru^{2+}$, DGDZVP full electron basis set was used [37]. The structures of $L^1$ and $L^2$ was fully optimized and the data were then used as the input for the optimization of $[RuL^1\ Cl(PPh_3)]^+$ and $[RuL^2Cl(PPh_3)]^+$. For the analysis of the molecular orbital contribution to the electronic absorption bands of the complexes, DFT–TDDFT technique was employed by using the Gaussian-09 program with the B3LYP exchange–correlation functional, and DGDZVP basis set to calculate the electronic transitions in gaseous state and also in solvent medium (in methanol as well as in $CH_2Cl_2$) to see the solvents effect [38].

### 2.4. Preparations of N,N′bis (benzimidazole-2yl-ethyl)ethylenediamine ($L^1$)

The ligand was synthesized by using the procedure reported elsewhere [39]. N,N′-bis(β-carbamolethyl)ethylenediamine (10.1 g, 0.05 M), which was prepared as reported elsewhere [40], was hydrolyzed by refluxing 3.0 h with NaOH (4 g, 0.1 M) in water (40 mL). After the neutralization of excess NaOH with HCl, then 1,2-diaminobenzene (10.8 g, 0.1 M) was added to the solution, and refluxed for 35 h in HCl solution (260 mL, 4 N). On cooling the solution mixture, the hydrochloride of the compound was obtained and then neutralized with aqueous ammonia. The crude product obtained was then re-crystallized from aqueous ethanol and dried over $P_2O_5$ vacuum. The spectral results of the compound agreed with the reported one: Elemental analysis, MS and NMR spectra for $L^1$ (0.80 g, 4.65%): Calc. for $C_{20}H_{24}N_6.5H_2O$: C, 54.77%, H, 7.81 y N, 19.16%. Found: C, 53.62%, H, 7.99%, N, 18.44%. MS, (ID, *m/z* (%)): MS: *m/z* = 349 (M + 1), 144 (100) $[C_9H_8N_2]^+$; $^1H$ NMR ($CD_3OD$): δ (ppm) = 2.80–3.31 (s, 4H, —N—$CH_2$—$CH_2$—N—), 4.91 (t, 8H, 2×Bzim —$CH_2$—CH2—), 7.18–7.48 (m, 8H, 2×Bzim-ring). $^{13}C$ NMR ($CD_3OD$): $^{13}C$ NMR ($CD_3OD$): δ (ppm) = 154.68 (HN—CH═N), 123.39–116.41 (benzimidazole ring), 49.99–48–29 (—$CH_2$—NH—$CH_2$), 29.98 (—$CH_2$—).

### 2.5. Ruthenium(II) complexes

#### 2.5.1. $[RuL^1Cl(PPh_3)]^+$

To a solution of $L^1$ (0.438 g, 1.0 mmol) dissolved in methanol (20.0 mL), a solution of $[RuCl_2(PPh_3)_3]$ (0.958 g, 1.0 mmol) dis-

**Table 1**
The optimized geometrical parameters (bond length (Å) and bond angles (°)) for the [Ru(II) $L^1Cl(PPh_3)$]Cl, [Ru(IV)$L^2Cl(PPh_3)$]Cl gaseous state ($L^1$ = *N,N′*-bis(benzimidazol-2yl-ethyl)ethylendiamine; $L^2$ = dianionic *N,N′*-bis(benzimidazol-2yl-ethyl)ethylendiamine).

| B3LYP/DGDZVP | | | B3LYP/DGDZVP | | |
|---|---|---|---|---|---|
| Bond length (Å) | $L^1$ | $L^2$ | Bond length (Å) | $[RuL^1Cl(PPh_3)]^+$ | $[RuL^2Cl(PPh_3)]^+$ |
| N(1)—C(2) | 1.315 | 1.315 | N(1)—Ru(1) | 2.184 | 2.231 |
| N(3)—C(2) | 1.386 | 1.384 | N(12)—Ru(1) | 2.221 | 2.005 |
| C(2)—C(10) | 1.498 | 1.502 | N(12′)—Ru(1) | 2.196 | 1.991 |
| C(11)—C(10) | 1.541 | 1.532 | N(1′)—Ru(1) | 2.217 | 2.245 |
| N(12)—C(11) | 1.466 | 1.469 | Cl(1)—Ru(1) | 2.504 | 2.445 |
| N(12)—C(13) | 1.471 | 1.498 | P(1)—Ru(1) | 2.434 | 2.556 |
| C(13)—C(13′) | 1.528 | 1.537 | *Bond Angle (°)* | | |
| N(12′)—C(13′) | 1.463 | 1.497 | N(1)—Ru(1)—N(12′) | 167.54 | 171.43 |
| N(12′)—C(11′) | 1.465 | 1.467 | N(1′)—Ru(1)—N(12) | 164.23 | 164.51 |
| C(11′)—C(10′) | 1.532 | 1.537 | Cl(1)—Ru(1)—P(1) | 178.54 | 177.67 |
| C(10′)—C(2′) | 1.501 | 1.499 | N(1)—Ru(1)—N(12) | 87.77 | 88.87 |
| N(1′)—C(2′) | 1.314 | 1.315 | N(1)—Ru(1)—N(1′) | 101.01 | 99.84 |
| N(3′)—C(2′) | 1.386 | 1.385 | N(12)—Ru(1)—N(12′) | 80.36 | 82.59 |
| | | | N(1′)—Ru(1)—N(12′) | 89.74 | 88.33 |
| | | | N(1)—Ru(1)—P(1) | 91.39 | 88.97 |
| | | | N(12)—Ru(1)—P(1) | 82.89 | 92.44 |
| | | | N(12′)—Ru(1)—P(1) | 92.96 | 92.11 |
| | | | N(1′)—Ru(1)—P(1) | 99.90 | 100.44 |
| | | | N(1)—Ru(1)—Cl(1) | 88.54 | 88.83 |
| | | | N(12)—Ru(1)—Cl(1) | 88.56 | 86.73 |
| | | | N(12′)—Ru(1)—Cl(1) | 87.409 | 89.95 |

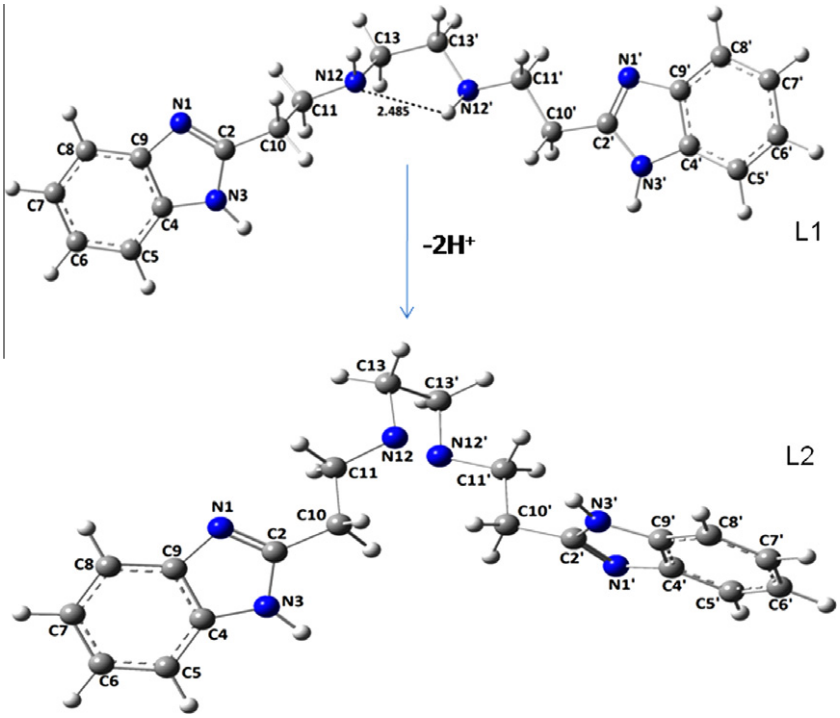


**Fig. 1.** Optimized structures of $L^1$ and $L^2$ in the gaseous state.

solved in methanol:$CH_2Cl_2$ (1:1, 30.0 mL) was added and the resulting solution was refluxed for 24 h. The solution was cooled to room temperature, and then concentrated by removing excess methanol via rotary evaporation. The residue obtained was washed with diethyl ether and then re-crystallized from methanol (20 mL). The greenish yellow solid was obtained (Yield: 0.81 g, 84%). Elemental analysis for $RuC_{38}H_{39}N_6Cl_2P$ (782): calcd. C 58.31, H 4.98, N 10.74; Found C 57.47, H 5.46, N 9.46. MS (FAB, *m*/*z* (%)): 747 ($M^+$, $C_{38}H_{39}N_6ClPRu$), 748 (M+1, $RuC_{36}H_{40}N_6ClP$), 262 ($C_9H_{11}N_3Ru$), 449 ($C_{20}H_{24}N_6Ru$), 485 ($C_{20}H_{24}N_6ClRu$). $^1H$ NMR ($CD_3OD$): $\delta$ = 2.15–3.34 (s, 4H, —N—$CH_2$—$CH_2$—N–), 4.88 (m, 8H, 2×Bzim —$CH_2$—$CH_2$—N), 7.54–7.64 (m, 2×Bzim-ring and of $PPh_3$). $^{13}C\{^1H\}$ NMR ($CD_3OD$): $\delta$ = 166.36 (NH—**C**H=N), 133.80–124.71 (Bzim-aromatic ring), 49.85 (—**C**$H_2$—**C**$H_2$ —). $31P\{^1H\}$ NMR ($CD_3OD$): $\delta$ = 33.33 ppm (s, P $(Ph)_3$). IR selected signals ($cm^{-1}$): 3393 (OH), 3233 (N—H), 1535 (C=N).

### 2.5.2. $[RuL^2Cl(PPh_3)]^+$

The molecular structure (Fig. 3b) of the complex was computationally constructed and then optimized to see dianionic effect in the spectral and spectral parameters.

## 3. Results and discussion

### 3.1. Geometrical analysis of $L^1$ & $L^2$ and their complexes $[RuL^1Cl(PPh_3)]^+$ and $[RuL^2Cl(PPh_3)]^+$

The ground state geometrical data for *N,N′*-bis (benzimidazole-2yl-ethyl)ethylendiamine ($L^1$) and its dianionic structure ($L^2$) are presented (Table 1 and Fig. 1). The results show that there is present an intra-molecular hydrogen bond N12—H···N12′ (2.48 Å) in the molecular structure of $L^1$ and the observed H-bond length (Fig. 1) is within the reported values 2.3–2.5 Å [41,42] and the distance is smaller than the sum of their van der Waals radii (1.5 Å for N and 1.1–1.2 Å for H). However, the H-bond disappeared when the ligand structure was de-protonated to give the $L^2$ structure. Furthermore, the charge distribution over the ligands, particularly on benzimidazole and amine was analyzed (Table 2). The results indicate that there is present an excess electron density over nitrogens (two $N_{Bzim}$ and two $N_{amine}$) that can facilitate bond formation with the metal. Besides, the hardness of the ligands, determined by (LUMO–HOMO)/2), [43,44] shows that the ligands can coordinate efficiently with $Ru^{2+}$ or $Ru^{4+}$. In the molecular orbital analysis, since the energy difference between HOMO and HOMO-1 (−0.14 eV for $L^1$; −0.24 eV for $L^2$) is very small, both orbitals can be involved cooperatively in the bond formation with the metal ions (Fig. 2). Thus, the orbitals HOMO and HOMO-1 are localized over N1—C2=N3 of benzimidazole ring that favor the formation of bonds with ruthenium ion.

It is known that Ru(II) has a 4*d* valence shell, which is more spatially extended than metals with a 3*d* valence shell, and forms low-spin complexes. In $[RuL^1(PPh_3)Cl]^+$, the Ru atom presents a

**Table 2**
Mulliken charges for [Ru(II) $L^1Cl(PPh_3)$]Cl, [Ru(IV)$L^2Cl(PPh_3)$]Cl gaseous state ($L^1$ = *N,N′*-bis(benzimidazol-2yl-ethyl)ethylendiamine; $L^2$ = dianionic *N,N′*-bis(benzimidazol-2yl-ethyl)ethylendiamine).

| Atoms | B3LYP/DGDZVP | | B3LYP/ DGDZVP | |
|---|---|---|---|---|
| | $L^1$ | $L^2$ | $[RuL^1Cl(PPh_3)]^+$ | $[RuL^2Cl(PPh_3)]^+$ |
| N(1) | −0.273 | −0.286 | −0.350 | −0.383 |
| N(12) | −0.493 | −0.192 | −0.622 | −0.358 |
| N(12′) | −0.470 | −0.184 | −0.605 | −0.345 |
| N(1′) | −0.279 | −0.272 | −0.354 | −0.374 |
| N(3) | −0.483 | −0.492 | −0.490 | −0.481 |
| N(3′) | −0.488 | −0.480 | −0.489 | −0.400 |
| C(2) | 0.233 | 0.294 | 0.340 | 0.363 |
| C(10) | −0.503 | −0.529 | −0.541 | −0.587 |
| C(11) | −0.278 | −0.281 | −0.342 | −0.388 |
| C(13) | −0.307 | −0.344 | −0.339 | −0.358 |
| C(13′) | −0.291 | −0.343 | −0.336 | −0.340 |
| C(11′) | −0.304 | −0.277 | −0.306 | −0.347 |
| C(10′) | −0.488 | −0.514 | −0.566 | −0.559 |
| C(2′) | 0.262 | 0.232 | 0.337 | 0.362 |
| Ru(1) | | | 0.519 | 0.677 |
| Cl(1) | | | −0.438 | −0.351 |
| P(1) | | | 0.533 | 0.565 |

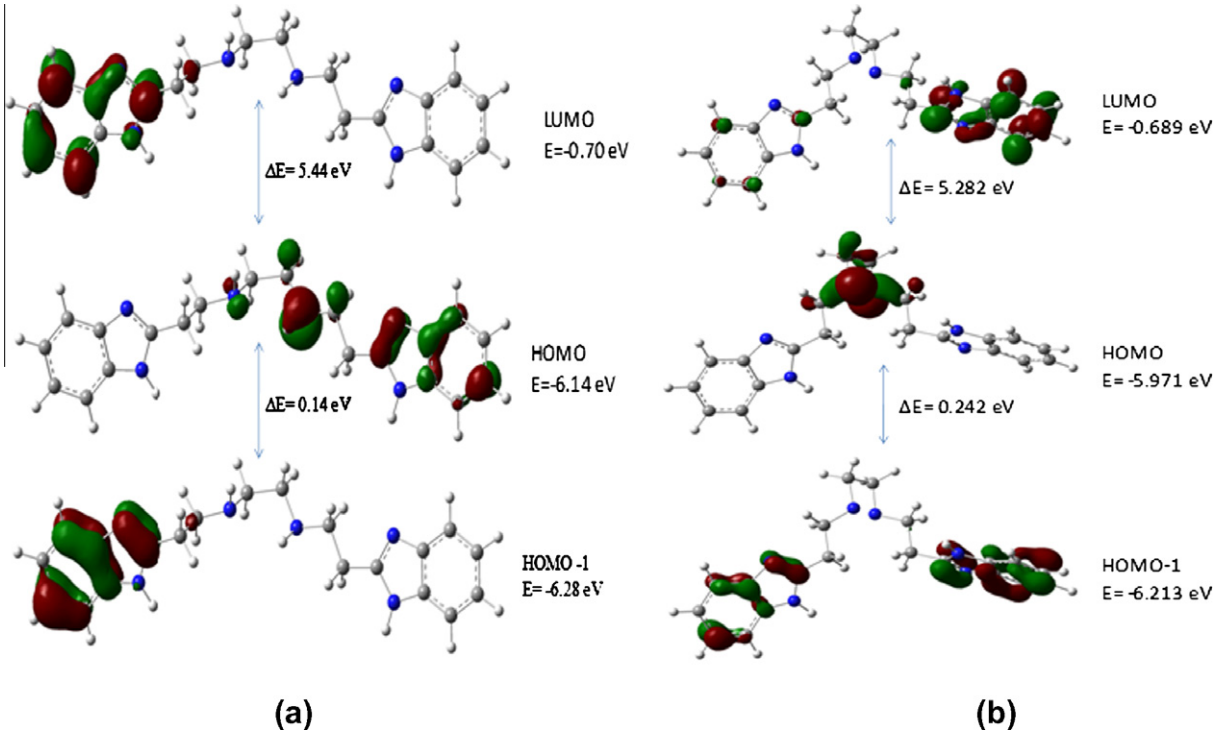


**Fig. 2.** Frontier molecular orbitals (HOMOs and LUMOs) analysis: (a) $L^1$; (b) $L^2$.

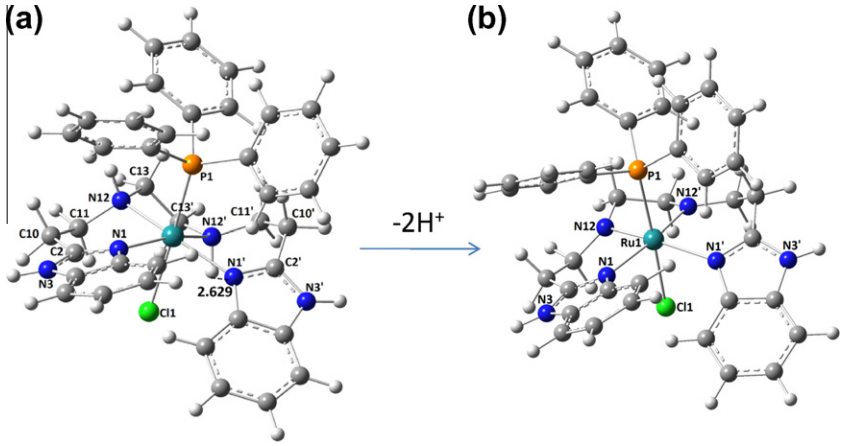


**Fig. 3.** Optimized structure of (a) $[RuL^1(PPh_3)Cl]^+$; (b) $[RuL^2(PPh_3)Cl]^+$ at gaseous state and in methanol.

+2 oxidation state with a low-spin of $4d^6\ 5s^0$ electronic configuration, which is relatively more stable than that of Ru(IV) having $4d^4\ 5s^0$ configuration. The structures of $[RuL^1Cl(PPh_3)]^+$ and $[RuL^2Cl(PPh_3)]^+$ are optimized and the results show (Fig. 3) that ligand $L^1$ is coordinated with ruthenium (II) ion in such a way that the metal ion exhibits a distorted octahedral geometry. In the structure, Ru(II) is bonded with two amines, and two benzimidazole nitrogens, forming an equatorial plane consisting of N(1), N(12), N(12′) and N(1′) atoms and their distances with the metal ion are: 2.184, 2.221, 2.196 and 2.217 Å respectively (Table 1); the axial bond lengths 2.434 Å for Ru(II)-P and 2.506 Å for Ru(II)-Cl were calculated from axially coordinated triphenyl phosphine P(1) and Cl(1) with the metal ion, agreeing with the published bond lengths [45]. According to Pearson's Principle of Hard and Soft Acids and Bases (HSAB) [46,47]: *Hard Acids prefer to bond with Hard Bases, and Soft Acids prefer to bond with Soft Bases.* The hard Ru(IV) cation reacts preferentially with a hard base such as

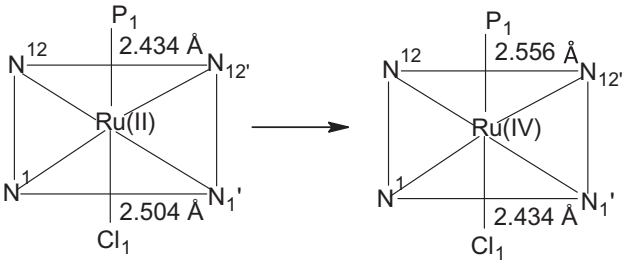


**Scheme 1.** Axial bond distance changes during Ru(II) oxidize to Ru(IV).

$N_{amine}$, or axial chloride ion, while soft Ru(II) bonds with soft base as $N_{bzim}$ (bzim = benzimidazole) or axial triphenyl phosphine. Hence there results shorter Ru(IV)—$N_{amine}$ or Ru(II)—$N_{bzim}$ distance compared to that of Ru(IV)—$N_{bzim}$ or Ru(II)—$N_{amine}$. Similarly, the

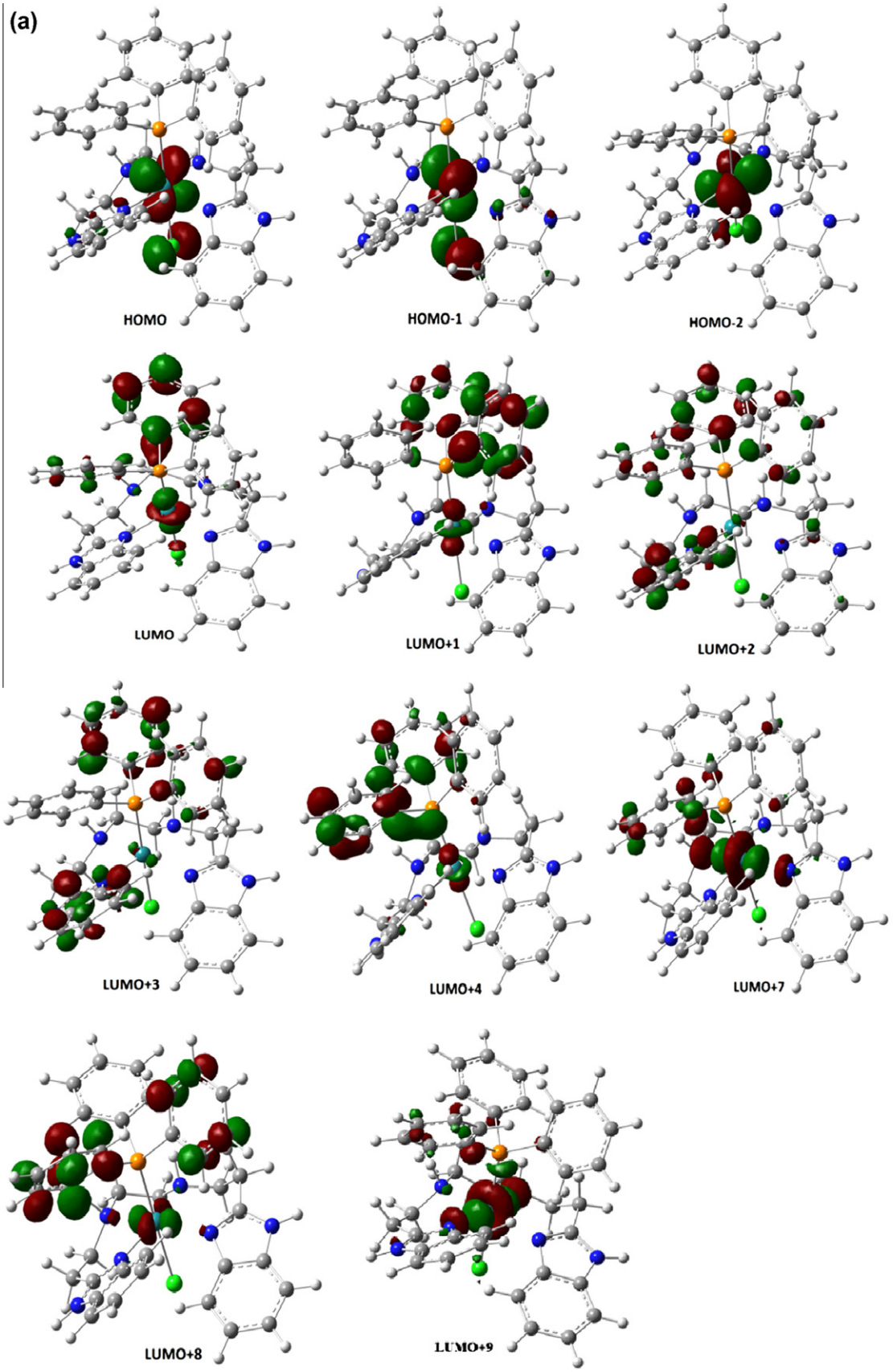


**Fig. 4.** Frontier molecular orbitals (HOMOs and LUMOs): (a) $[RuL^{1}(PPh_3)Cl]^{+}$; (b) $[RuL^{2}(PPh_3)Cl]^{+}$ .

hard nature of $Cl^{-}$ causes it to coordinate with Ru(IV), while the soft nature of triphenylphosphine makes it interact with Ru(II), resulting in smaller distances for Ru(IV)—Cl or Ru(II)—P bonds than for Ru(II)—Cl or Ru(IV)-P (see data and Scheme 1 given below):

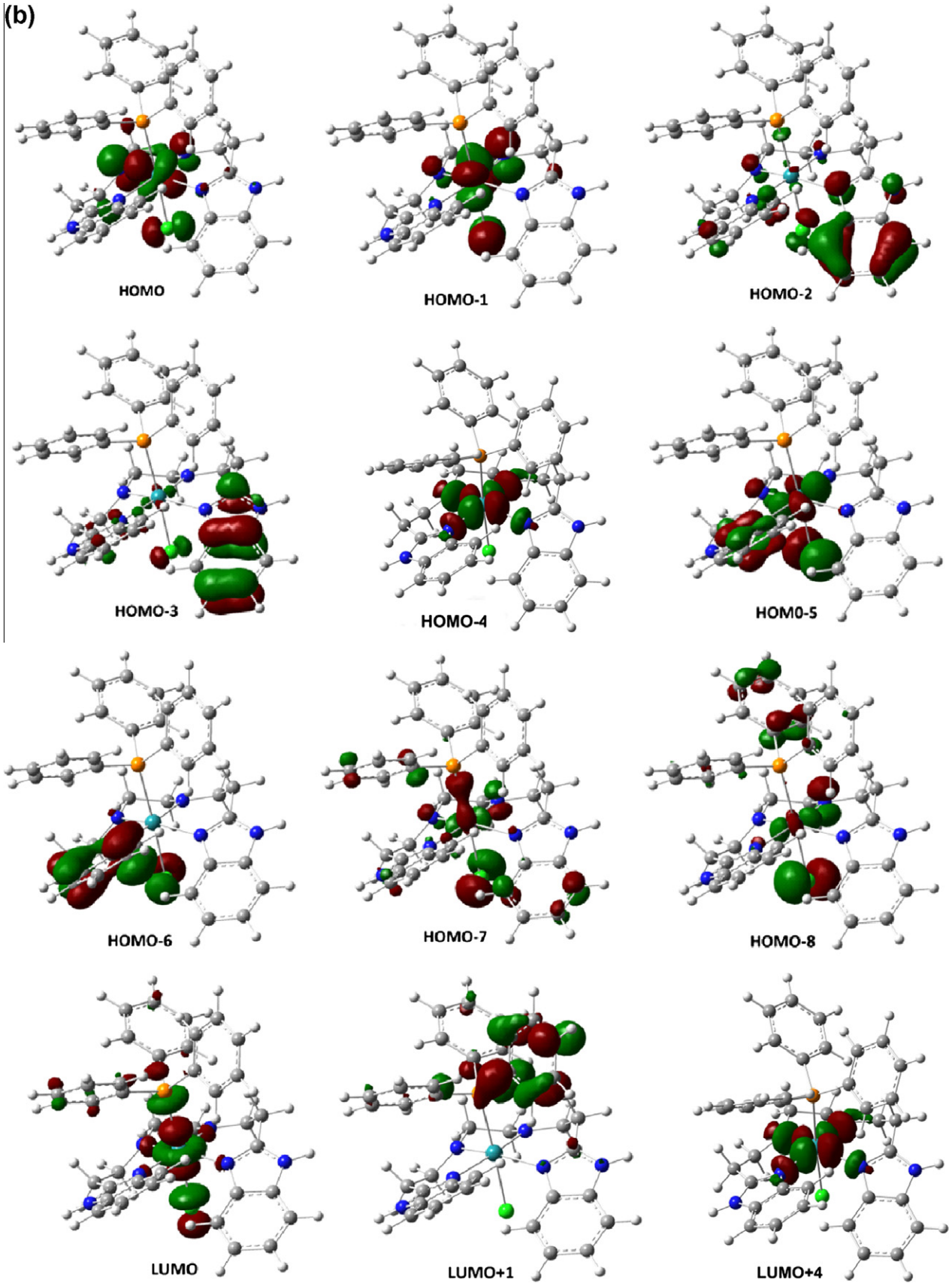


**Fig. 4** (*continued*)

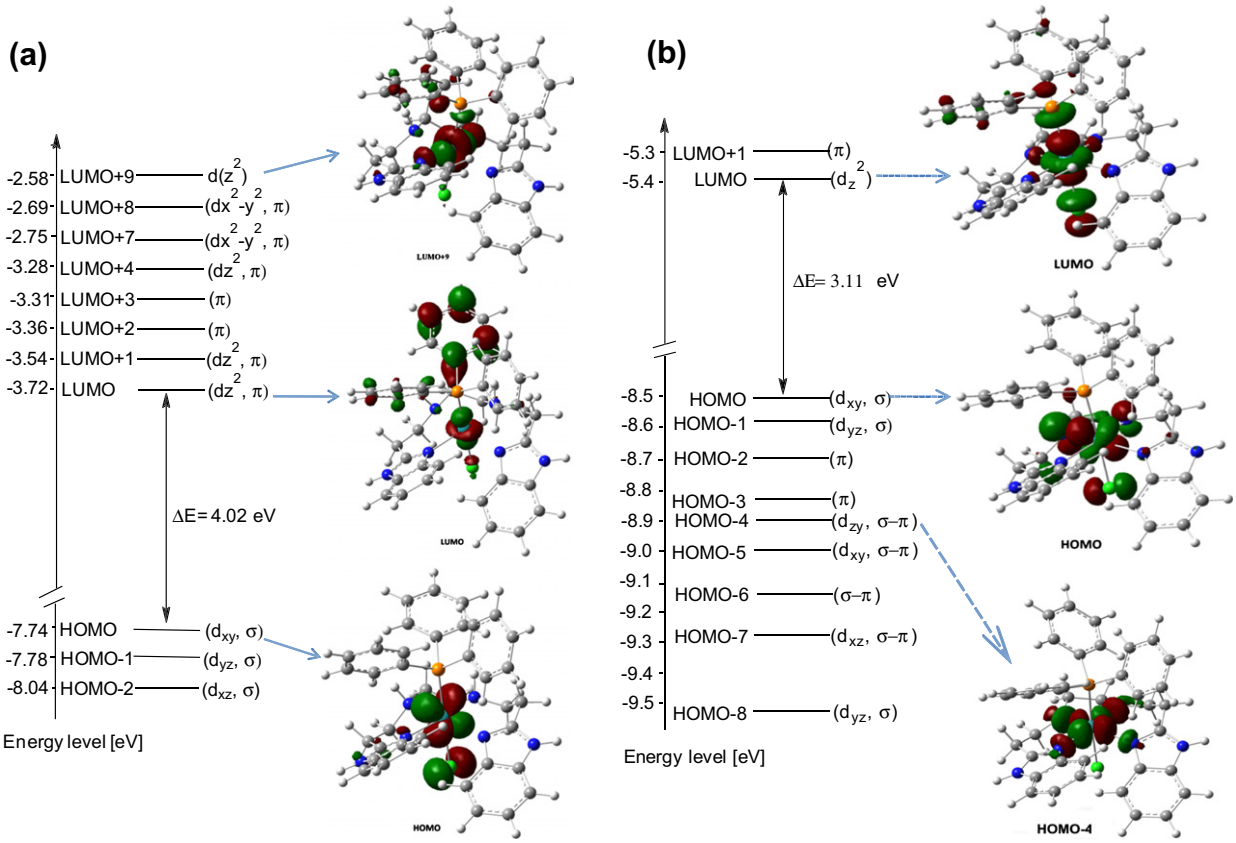


**Fig. 5.** Frontier molecular orbital energy level diagram of (a) $[RuL^1(PPh_3)Cl]^+$; (b) $[RuL^2(PPh_3)Cl]^+$ .

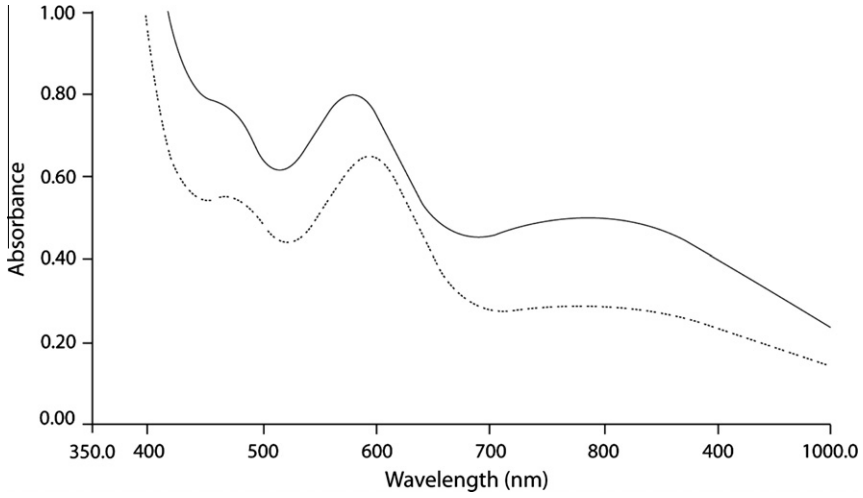


**Fig. 6.** Electronic spectra of $[RuL^1(PPh_3)Cl]^+$: in $CH_2Cl_2$ (. . ..) and in methanol (-).

Ru(II)—$N_{bzim}$ (2.184 Å) <
**Soft–soft**
Ru(II)—P (2.434 Å) <
**Soft–soft**
Ru(IV)—$N_{bzim}$ (2.231 Å) >
Hard–soft
Ru(II)—Cl (2.504 Å) >
Soft–hard

Ru(II)—$N_{amine}$ (2.221 Å)
Soft–hard
Ru(IV)—P(2.556 Å)
Hard–soft
Ru(IV)—$N_{amine}$(2.005 Å)
**Hard–hard**
Ru(IV)—Cl (2.445 Å)
**Hard–hard**

The obtained bond distances (2.184–2.221 Å for Ru(II)—N) of the complex fall approximately in the range of those reported for the ruthenium (II) complexes containing benzimidazoles [48,49]. The resulting bond angles for *trans* bonded atoms around the metal center are: 167.54° for N(1)—Ru(1)—N(12′), 164.23° for N(1′)—Ru(1)—N(12), and 178.54° for Cl(1)—Ru(1)—P(1) and other bond angles are in the range of 80.36° to 101.01°, showing that the metal presents a distorted octahedral structure. This is consistent with the published crystal structures of the other metals Cu(II), Ni(II) with the present ligand $L^1$ that favors the formation of distorted octahedral geometry. For the case of $[RuL^2Cl(PPh_3)]^+$, a strong interaction between N12 or N12′ with $Ru^{4+}$ is expected; thus, a smaller bond distance for Ru(IV)—N—(12) (2.005 Å) or

**Table 3**
TDDFT spectral data of electronic transitions [Ru(II) $L^1Cl(PPh_3)$]Cl, [Ru(IV)$L^2Cl(PPh_3)$]Cl gaseous state ($L^1$ = *N,N′*-bis(benzimidazol-2yl-ethyl)ethylendiamine; $L^2$ = dianionic *N,N′*-bis(benzimidazol-2yl-ethyl)ethylendiamine) with oscillator strength $f > 0.0011$.

| W(nm) | Osc. Strength (f) | Composition | Character | Theory (nm) |
|---|---|---|---|---|
| *[RuL¹Cl(PPh₃)]⁺* | | | | |
| 473.3 | 0.0022 | HOMO → LUMO (29%) | MLCT | 471.43 |
| | | HOMO-1 → LUMO + 1 (4%) | | |
| | | HOMO-1 → LUMO + 7 (3%) | | |
| | | HOMO-1 → LUMO + 9 (2%) | | |
| 437.94 | 0.0011 | HOMO-2 → LUMO + 7(31%) | MLCT | |
| | | HOMO-2 → LUMO + 8 (9%) | | |
| | | HOMO → LUMO + 7 (9%) | | |
| | | HOMO → LUMO + 8 (3%) | | |
| | | HOMO-2 → LUMO + 3 (3%) | | |
| 351.2 | 0.0021 | HOMO → LUMO + 1 (49%) | | |
| | | HOMO → LUMO (33%) | | |
| | | HOMO → LUMO + 7 (6%) | | |
| | | HOMO → LUMO + 3 (3%) | | |
| | | HOMO → LUMO + 4 (2%) | | |
| 348.21 | 0.0039 | HOMO-1 → LUMO + 1(46%) | | |
| | | HOMO-1 → LUMO (41%) | | |
| | | HOMO-1 → LUMO + 7 (4%) | | |
| | | HOMO-1 → LUMO + 3 (2%) | | |
| 335.13 | 0.0025 | HOMO → LUMO + 2 (43%) | MLCT | 335.71 |
| | | HOMO → LUMO + 1 (14%) | | |
| | | HOMO-1 → LUMO + 2 (3%) | | |
| 328.77 | 0.0159 | HOMO → LUMO + 2 (35%) | | |
| | | HOMO → LUMO + 4 (20%) | | |
| | | HOMO → LUMO + 3 (13%) | | |
| | | HOMO → LUMO + 9 (4%) | | |
| *[RuL²Cl(PPh₃)]⁺* | | | | |
| 654.67 | 0.0143 | HOMO-1 → LUMO (80%) | MLCT | 625.00 |
| | | HOMO-6 → LUMO (6%) | | |
| | | HOMO-3 → LUMO (5%) | | |
| 609.08 | 0.0025 | HOMO → LUMO+1 (78%) | MLCT | |
| | | HOMO-3 → LUMO (4%) | | |
| 596.72 | 0.0057 | HOMO-3 → LUMO (51%) | MLCT | |
| | | HOMO-6 → LUMO (8%) | | |
| 572.19 | 0.0016 | HOMO-4 → LUMO (42%) | MLCT | |
| | | HOMO-3 → LUMO (26%) | | |
| | | HOMO-8 → LUMO (4%) | | |
| 538.19 | 0.0123 | HOMO-6 → LUMO (42%) | MLCT | 525.00 |
| | | HOMO-4 → LUMO (20%) | | |
| | | HOMO-7 → LUMO (2%) | | |
| 523.17 | 0.0043 | HOMO-5 → LUMO (56%) | MLCT | |
| | | HOMO-7 → LUMO(30%) | | |
| | | HOMO-6 → LUMO (7%) | | |
| | | HOMO-8 → LUMO (4%) | | |
| 504.95 | 0.024 | HOMO-7 → LUMO (45%) | MLCT | |
| | | HOMO-3 → LUMO (3%) | | |

*Note*: For $[RuL^1Cl(PPh_3)]^+$, experimental electronic bands observed were: 791 nm (555), 581 nm (870), 465 nm (823); $\varepsilon \times 10^{-4}$, $M^{-1}\,cm^{-1}$ is presented in the parenthesis.

Ru(IV)—N—(12′) (1.991 Å) is obtained than that for Ru(IV)—N(1) (2.231 Å) or Ru(IV)—N(1′) (2.245 Å). However, the dihedral angles obtained for the complex are almost similar to the angles resulted for $[RuL^1Cl(PPh_3)]^+$.

Furthermore, having analyzed the electronic charge density of the ligands and the ruthenium(II) complexes calculated by the Mullikan method, it was found there is a considerable change in the charge density of the donor atoms of the ligands after the formation of the complexes (Table 2). For example, for the $L^1$, the charge densities were: N1 (−0.273), N12 (−0.493), N12′ (−0.470), and N1′ (−0.279); however, after its complex formation with Ru(II), the values were changed to −0.350, −0.622, −0.605, and −0.354. It appears that there is a steep change in the values for the coordinated nitrogens because of the charge transfer from ligand to metal during the complex formation. A similar charge transfer was also observed during the complex formation of dianionic $L^2$ with Ru(IV), i.e., the charges of N1 (−0.286), N12 (−0.192), N12′ (−0.184), and N1′ (−0.272) were changed to −0.383, −0.358, −0.345, and −0.374 after the complex formation with Ru(IV). Also, it was observed that the charges were moved from 0.519 for Ru(II) to 0.677 for Ru(IV).

In addition, molecular orbital (MO) analysis establishes the formation of bonds through the energy stabilization of the orbitals of rutheniumr(II) with those of ligands; all low-lying HOMOs result from the overlap of the metal and ligand orbitals. For instance, for $[RuL^2Cl(PPh_3)]^+$, the HOMOs orbitals were obtained through the combinations of *d* [Ru(IV)] with the *p* orbitals of $L^2$; the orbitals (HOMO to HOMO-*x*; $x = 1–8$) (Figs. 4b and 5b) resulted from the mixing of the *d* orbital (metal) with $\pi/p$ of the ligand, where $L^1$ contributes considerably to the $\pi/p$ character of Ru(II), the LUMO being derived through the combination of the $\pi*$ type [N(1), N(12), N(12′) N(1′)] of ligands with *d* (Ru ion). The LUMO is being generated because of the $d_z^2$ (Ru) mixture with the orbitals of atoms [N(1), N(12), N(12′), N(1′), P(1) and Cl(1)], and thus confirms the existence of a Ru—P bond in the geometry. Moreover, the π-character of the benzimidazole moiety presented in the complex was corroborated: the HOMO, and other low-lying orbitals (HOMO-*x* ($x = 1–8$) for $RuL^{22+}$ were observed. Similarly, the HOMOs orbitals were obtained through the combinations of *d* [Ru(II)] with the *p* orbitals of $L^1$ for $[RuL^1Cl(PPh_3)]^+$ (Figs. 4a and 5a).

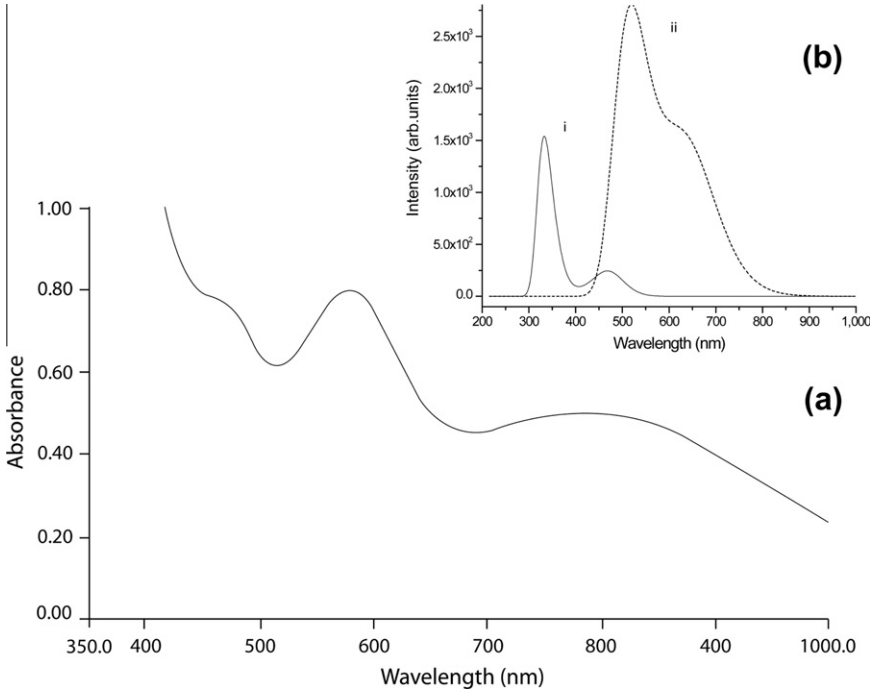


**Fig. 7.** a) Experimental absorption spectra in methanol; b) TD-DFT spectra: (i) $[RuL^1(PPh_3)Cl]^+$; (ii) $[RuL^2(PPh_3)Cl]^+$.

### 3.2. Electronic absorption spectra

The absorption spectra of $[RuL^1(PPh_3)Cl]^+$ recorded in different solvents (Fig. 6) show that there is present a solvent effect in the absorption spectra; for example, the absorption spectrum measured for the complex in $CH_2Cl_2$ is red shifted when compared to that observed in methanol. For $[RuL^1Cl(PPh_3)]Cl$, the spectrum in the visible region is dominated by the metal- to- ligand charge-transfer (MLCT, $d \rightarrow \pi^*$) bands: 790.6 nm (Ru(II) $d \rightarrow$ benzimidazole), 581.3 nm (Ru(II) $d \rightarrow$ P($Ph_3$) and, 465.4 (amine N $\rightarrow$ $d$ Ru(II)) (Table 3). Furthermore, in the complex, both processes i.e., an electron donation from the σ orbital of the ligand toward an empty $d$ orbital of the metal and a simultaneous donation from a filled $d$ orbital to a $\pi^*$ anti-bonding orbital of the ligand, promote each other for the visible bands. Since the ligand $L^1$ has σ donor orbitals localized on N and π-donor and $\pi^*$-acceptor orbitals delocalized on benzimidzole rings, the back-donation between the ligand and the Ru orbitals is significant. The strongest absorption in the UV region can be assigned as an intraligand $\pi-\pi^*$ transitions.

### 3.3. TD–DFT absorption spectrum

Since the visible bands of $[RuL^1(PPh_3)Cl]^+$ in methanol were broad, TD–DFT was then used to analyze the orbital contributions to the MLCT spectral bands. The calculated absorption spectrum of the complex is shown in Fig. 7 and the most representative calculated optical transitions being presented Table 3. The calculated spectrum qualitatively agrees only with the high energy bands of the experimental spectra (i.e., peaks ≈465 nm and ≈350 nm), however, other visible bands (580 and 790 nm), that were observed in the experimental spectra, did not appear in the calculated spectra. The TD-DFT of $[RuL^2(PPh_3)Cl]^+$, where the ligand is presented in dianionic form and Ru ion is at +4 oxidation state, is red-shifted compared to the calculated spectrum of $[RuL^1(PPh_3)Cl]^+$ and almost matches the visible experimental bands. Although the presence of Ru-complex of ligand $L^1$ is confirmed in the solution by spectral electrochemical methods, the existence of its de-protonated $L^2$ with Ru(IV) in the solution is unable to be confirmed by those methods. However, there is a significant variation for the protonated and de-protonated Ru complexes in the calculated electronic spectra [50]. In addition to the de-protonated effect, the solvent effect is also associated with the absorption bands. Thus, the MLCT band observed at 790.6 nm in methanol is shifted to 654.7 nm in the TD-DFT spectrum of $[RuL^2(PPh_3)Cl]^+$. In a previous report [38], the contribution of Ru $d$ orbital with the ligand orbital was analyzed, for instance, in Ru(II) complexes $[Ru(H_3\text{-tctpy})(NCS)_3]^{-1}$ and $[Ru(H_3\text{-tctpy})(SCN)_3]^{-1}$ ($H_3$-tctpy = 4,4′,4″-tricarboxy-2,2′:6,2″-terpyridine), the contribution of $d$ orbital mixed with ligand orbital in solvent was explained; for $[Ru(H_3\text{-tctpy})(NCS)_3]^{-1}$, where both axial position are occupied by NCS, a lower contribution of d orbital in solvent (94% in ethanol, 98% in gaseous phase) was reported; while in $[Ru(H_3\text{-tctpy}))(SCN)_3]^{-1}$, where SCN are coordinated in both axial positions, a higher contribution of $d$ orbital in solvent (88% in ethanol than 83% in gas phase) was observed. Therefore, the main absorption features of the experimental spectrum are reproduced by theory despite having a red shift in the lowest-energy band in the visible region. In addition, it was seen that there is present a solvent effect in the DFT–TD electronic spectra, i.e., the spectral bands of $[RuL^1Cl(PPh3)]Cl$ (473, 437, 351 and 348 nm) at gaseous state are slightly moved to 477, 436, 360 and 349 nm in methanol included calculated spectra (see Supplementary materials). It appears that the transitions originate from the HOMO-$x$ ($x$ = 0, 1, 3, 4, 6 and 8) (Ru—$N_{bzim}$) couple to the LUMO or LUMO + 1) at 654.7, 609.1, 596.7 and 572.2 nm. We therefore see that the lowest-energy band in the visible region is derived from an excited state of mixed Ru(IV)—N, i.e., HOMOs localized on the ligand, especially on the benzimidazole and amine moieties considerably overlap with the LUMO of metal ion through MLCT. At shorter wavelengths (538.2 and 505.03 nm) the positions are in near agreement with the experimental values of 581.2 nm and 465.3 nm with a difference of 40 to 60 nm; the bands (538.2, 523.2 nm and 505.0 nm) are due to three electronic transitions of mixed MLCT character from HOMO-$x$ ($x$ = 3, 4, 5, 6, 7 and 8) to the higher-lying LUMO orbitals ($d_z^2$). Similarly, other mixed MLCT transitions are from the orbitals HOMO-$x$ ($x$ = 3 and 7) to $d_{xy}$ character of LUMO, and appear at 465 nm in methanol and at 505 nm in the

TDDFT with a sizable intensity. It shows that in the frontier orbitals for the ground state of the complex, the HOMOs have a significant contribution from Ru $t_{2g}$ *d*-orbital with a π contribution from the benzimidazole. The HOMO of the complex consists mainly of an anti-bonding combination of a $t_2$g orbital on Ru ion and a *p* orbital on $Cl^-$.

## 4. Conclusion

DFT and TD–DFT studies show that the complex $[Ru(L^1)Cl(PPh_3)]Cl$ is present in distorted octahedral geometry, where since the ligand $L^1$ has σ donor orbitals localized on N and π-donor, and $\pi^*$-acceptor orbitals delocalized on benzimidzole rings, the back-donation between the ligand and the Ru orbitals is significant in the absorption spectra. This is the reason why in the spectra, three MLCT bands are observed in methanol while in the calculated absorption spectra only two clear bands associated with six MLCT electronic transitions are noticed. Furthermore, DFT TDDFT was used to analyze the molecular orbitals contribution to MLCT bands that resulted in the visible region, showing that the calculated spectrum of $[RuL^1Cl(PPh_3)]^+$ qualitatively agrees with high energy bands of the experimental spectrum, while other visible bands (≈580 and 790 nm) in the experimental spectrum approximately coincide with the TD–DFT of $[RuL^2(PPh_3)Cl]^+$; however, the existence of Ru(IV)L2 in the solution is not confirmed. Additionally, the molecular orbital HOMOs are localized over the benzimidazole and amine moieties that favor a strong bond with the metal ion.

## Acknowledgements

The authors acknowledge the Direccíon General de Asuntos del Personal Académico (Project PAPIIT No. IN226310 for economic support. We also thank DGSCA-UNAM for the computation facilities.

## Appendix A. Supplementary material

Supplementary data associated with this article can be found, in the online version, at doi:10.1016/j.molstruc.2011.01.005.

## References

[1] F. Frausin, M. Cocchietto, A. Bergamo, V. Searcia, A. Furlani, G. Sava, Cancer Chemother. Pharmacol. 50 (2002) 405.
[2] B. Serli, E. Zangrando, T. Gianfeffara, L. Yellowlees, E. Alessio, Coord. Chem. Rev. 245 (2003) 73.
[3] I. Turel, M. Pecanac, A. Golobic, E. Alessio, B. Serli, A. Bergamo, J. Inorg. Biochem. 96 (2003) 241.
[4] M.J. Clarke, F.C. Zhu, D.R. Frasca, Chem. Rev. (Washington, DC, US) 99 (1999) 2511.
[5] L. Prodi, F. Bolletta, M. Montalti, N. Zaccheroni, Coord. Chem. Rev. 205 (2000) 59.
[6] M. Gratzel, Nature 414 (2001) 338.
[7] B. Oregan, M. Gratzel, Nature 353 (1991) 737.
[8] N. Vlachopoulos, P. Liska, J. Augustynski, M. Gratzel, J. Am. Chem. Soc. 110 (1988) 1216.
[9] W.I. Sundquist, S.J. Lippard, Coord. Chem. Rev. 100 (1990) 293.
[10] M. Cusumano, Inorg. Chem 37 (1998) 563.
[11] D.S. Sigman, A. Mazumder, D.M. Perrin, Chem. Rev. (Washington, DC, US) 93 (1993) 2295.
[12] H.Q. Liu, T.C. Cheung, S.M. Peng, C.M. Che, J. Chem. Soc. Chem. Commun (1995) 1787.
[13] H.Q. Liu, S.M. Peng, C.M. Che, J. Chem. Soc. Chem. Commun (1995) 509.
[14] F. Frausin, V. Scarcia, M. Cocchietto, A. Furlani, B. Serli, E. Alessio, G. Sava, J. Pharmacol. Exp. Ther. 313 (2005) 227.
[15] M. Cocchietto, G. Sava, Pharmacol. Toxicol. 87 (2000) 193.
[16] R.E. Aird, J. Cummings, A.A. Ritchie, M. Muir, R.E. Morris, H. Chen, P.J. Sadler, D.I. Jodrell, Br. J. Cancer 86 (2002) 1652.
[17] R.E. Morris, R.E. Aird, P.D. Murdoch, H.M. Chen, J. Cummings, N.D. Hughes, S. Parsons, A. Parkin, G. Boyd, D.I. Jodrell, P.J. Sadler, J. Med. Chem. 44 (2001) 3616.
[18] J.B. Asbury, R.J. Ellingson, H.N. Ghosh, S. Ferrere, A.J. Nozik, T.Q. Lian, J. Phys. Chem. B 103 (1999) 3110.
[19] N.G. Park, M.G. Kang, K.M. Kim, K.S. Ryu, S.H. Chang, D.K. Kim, J. Van de Lagemaat, K.D. Benkstein, A.J. Frank, Langmuir 20 (2004) 4246.
[20] T.A. Heimer, E.J. Heilweil, C.A. Bignozzi, G.J. Meyer, J. Phys. Chem. A 104 (2000) 4256.
[21] M.K. Nazeeruddin, R. Humphry-Baker, P. Liska, M. Gratzel, J. Phys. Chem. B 107 (2003) 8981.
[22] M.K. Nazeeruddin, F. De Angelis, S. Fantacci, A. Selloni, G. Viscardi, P. Liska, S. Ito, B. Takeru, M.G. Gratzel, J. Am. Chem. Soc. 127 (2005) 16835.
[23] M.K. Nazeeruddin, C. Klein, P. Liska, M. Gratzel, Coord. Chem. Rev. 249 (2005) 1460.
[24] J. Bisquert, D. Cahen, G. Hodes, S. Ruhle, A. Zaban, J. Phys. Chem. B 108 (2004) 8106.
[25] M.K. Nazeeruddin, A. Kay, I. Rodicio, R. Humphrybaker, E. Muller, P. Liska, N. Vlachopoulos, M. Gratzel, J. Am. Chem. Soc. 115 (1993) 6382.
[26] M.K. Nazeeruddin, P. Pechy, M. Gratzel, Chem. Commun. (Cambridge, UK) (1997) 1705.
[27] A. Juris, V. Balzani, F. Barigelletti, S. Campagna, P. Belser, A. Vonzelewsky, Coord. Chem. Rev. 84 (1988) 85.
[28] T. Pandiyan, M. Palaniandavar, M. Lakshminarayanan, H. Manohar, J. Chem. Soc. Dalton Trans. (1992) 3377.
[29] M. Palaniandavar, T. Pandiyan, M. Lakshminarayanan, H. Manohar, J. Chem. Soc. Dalton Trans. (1995) 455.
[30] T. Pandiyan, K. Panneerselvam, M. SorianoGarcia, C.D. deBazua, E.M. Holt, Acta Crystallogra. Sect. C 52 (1996) 1137.
[31] G.A. van Albada, I. Mutikainen, U. Turpeinen, J. Reedijk, J. Chem. Crystallogr. 37 (2007) 489.
[32] A.W. Addison, H.M.J. Hendriks, J. Reedijk, L.K. Thompson, Inorg. Chem. 20 (1981) 103.
[33] T. Pandiyan, J.G. Hernandez, N.T. Medina, S. Bernes, Inorg. Chim. Acta 357 (2004) 2570.
[34] M.J. Frisch, G.W. Trucks, H.B. Schlegel, G.E. Scuseria, M.A. Robb, J.R. Cheeseman, J.A. Jr. Montgomery, T. Vreven, K.N. Kudin, J.C. Burant, J.M. Millam, S.S. Iyengar, J. Tomasi, V. Barone, B. Mennucci, M. Cossi, G. Scalmani, N. Rega, G.A. Petersson, H. Nakatsuji, M. Hada, M. Ehara, K. Toyota, R. Fukuda, J. Hasegawa, M. Ishida, T. Nakajima, Y. Honda, O. Kitao, H. Nakai, M. Klene, X. Li, J.E. Knox, H.P. Hratchian, J.B. Cross, C. Adamo, J. Jaramillo, R. Gomperts, R.E.Stratmann, O. Yazyev, A.J. Austin, R. Cammi, C. Pomelli, J.W. Ochterski, P.Y. Ayala, K. Morokuma, G.A.Voth, P. Salvador, J.J. Dannenberg, V.G. Zakrzewski, S. Dapprich, A.D. Daniels, M.C. Strain, O. Farkas, D.K. Malick, A.D. Rabuck, K. Raghavachari, J.B. Foresman, J.V. Ortiz, Q. Cui, A.G. Baboul, S. Clifford, J. Cioslowski, B.B. Stefanov, G. Liu, A. Liashenko, P. Piskorz, I. Komaromi, R.L. Martin, D.J. Fox, T. Keith, M.A. Al-Laham, A.N.C.Y. Peng, M. Challacombe, P.M.W. Gill, B. Johnson, W. Chen, M.W. Wong, C. Gonzalez, J.A. Pople Gaussian, Revision D 01; Gaussian Inc., Wallingford, CT, 2004.
[35] A.D. Becke, Phys. Rev. A 38 (1988) 3098.
[36] C.T. Lee, W.T. Yang, R.G. Parr, Phys. Rev. B 37 (1988) 785.
[37] N. Godbout, D.R. Salahub, J. Andzelm, E. Wimmer, Can. J. Chem. 70 (1992) 560.
[38] S. Ghosh, G.K. Chaitanya, K. Bhanuprakash, M.K. Nazeeruddin, M. Gratzel, P.Y. Reddy, Inorg. Chem. 45 (2006) 7600.
[39] U. Sivagnanam, T. Pandiyan, M. Palaniandavar, Indian J. Chem. Sect. B 32 (1993) 572.
[40] M.S. Chao, C.S. Chung, J. Chem. Soc. Dalton Trans. (1981) 683.
[41] R. Taylor, O. Kennard, J. Am. Chem. Soc. 104 (1982) 5063.
[42] G.R. Desiraju, T. Steiner, The Weak Hydrogen Bond in Structural Chemistry and Biology, Oxford University Press, Inc., New York, 1999.
[43] R.G. Pearson, Inorg. Chim. Acta 270 (1998) 252.
[44] R.G. Pearson, J. Chem. Ed. 76 (1999) 267.
[45] D. Mishra, A. Barbieri, C. Sabatini, M.G.B. Drew, H.M. Figgle, W.S. Sheldrick, S.K. Chattopadhyay, Inorg. Chim. Acta 360 (2007) 2231.
[46] R.G. Pearson, J. Am. Chem. Soc. 85 (1963) 3533.
[47] R.G. Pearson, J. Chem. Educ. 45 (1968) 581.
[48] D. Saha, S. Das, C. Bhaumik, S. Dutta, S. Baitalik, Inorg. Chem. 49 (2010) 2334.
[49] C. Bhaumik, S. Das, D. Saha, S. Dutta, S. Baitalik, Inorg. Chem. 49 (2010) 5049.
[50] C. Barolo, M.K. Nazeeruddin, S. Fantacci, D. Di Censo, P. Comte, P. Liska, G. Viscardi, P. Quagliotto, F. De Angelis, S. Ito, M. Gratzel, Inorg. Chem. 45 (2006) 4642.